


rhIL-7-hyFc and hIL-2/TCB2c combination promotes an immune-stimulatory tumor microenvironment that improves antitumor efficacy of checkpoint inhibitors

Minji Lee ¹, Sun-Kyoung Im,¹ Seungtae Baek,¹ Mankyu Ji,¹ Miyoung Kim,¹ Eun Ju Lee,¹ Seung Taek Ji,¹ Sara Ferrando-Martinez,² Alexandra Wolfarth,² Jun-Young Lee,³ Daeun Kim,³ Donghoon Choi¹

To cite: Lee M, Im S-K, Baek S, et al. rhIL-7-hyFc and hIL-2/TCB2c combination promotes an immune-stimulatory tumor microenvironment that improves antitumor efficacy of checkpoint inhibitors. *Journal for ImmunoTherapy of Cancer* 2024;12:e008001. doi:10.1136/jitc-2023-008001

► Additional supplemental material is published online only. To view, please visit the journal online (<https://doi.org/10.1136/jitc-2023-008001>).

Accepted 06 February 2024



© Author(s) (or their employer(s)) 2024. Re-use permitted under CC BY-NC. No commercial re-use. See rights and permissions. Published by BMJ.

¹Research Institute of NeoImmuneTech, Co., Ltd, Pohang, Korea (the Republic of)
²NeoImmuneTech, Inc, Rockville, Maryland, USA
³Selecixine, Pohang, Korea (the Republic of)

Correspondence to

Dr Donghoon Choi;
dhchoi@neoimmunetech.com

ABSTRACT

Background Recombinant human interleukin (rhIL)-7-hyFc (efineptakin alfa; NT-17) is a potent T-cell amplifier, with two IL-7 molecules fused to IgD/IgG4 elements. rhIL-7-hyFc promotes extensive infiltration of CD8⁺ T cells into the tumor, concurrently increasing the numbers of intratumoral PD-1⁺CD8⁺ T cells. The hIL-2/TCB2 complex (SLC-3010) inhibits tumor growth by preferential activation of CD122 (IL-2Rβ)^{high} CD8⁺ T cells and natural killer cells, over regulatory T cells (Tregs). We investigated the underlying mechanisms of rhIL-7-hyFc and hIL-2/TCB2c antitumor activity and the potential synergistic efficacy, specifically focusing on tumor-specific CD8⁺ cells within the tumor and the tumor-draining lymph nodes (tdLN).

Methods MC38 and CT26 tumor-bearing mice were administered with 10 mg/kg rhIL-7-hyFc intramuscularly and 0.9 mg/kg hIL-2/TCB2c intravenously. Anti-PD-1 monoclonal antibody was administered intraperitoneally three times at 3-day intervals at a dose of 5 mg/kg. Tumor volume was measured to assess efficacy. To compare the composition of immune cells between each monotherapy and the combination therapy, we analyzed tumors and tdLNs by flow cytometry.

Results Our data demonstrate that the combination of rhIL-7-hyFc and hIL-2/TCB2c increases efficacy and generates an immune-stimulatory tumor microenvironment (TME). The TME is characterized by an increased infiltration of tumor-specific CD8⁺ T cells, and a decreased frequency of CD39^{high}TIM3⁺Treg cells. Most importantly, rhIL-7-hyFc increases infiltration of a CD62L⁺Ly108⁺ early progenitor population of exhausted CD8⁺ T cells (T_{PEX}), which may retain long-term proliferation capacity and replenish functional effector CD8⁺ T cells. hIL-2/TCB2c induces differentiation of CD62L⁺Ly108⁺ T_{PEX} rapidly into CD101⁺ terminally differentiated subsets (terminally exhausted T cell (T_{EX term})). Our study also demonstrates that rhIL-7-hyFc significantly enhances the proliferation rate of T_{PEX} in the tdLNs, positively correlating with their abundance within the tumor.

WHAT IS ALREADY KNOWN ON THIS TOPIC

⇒ Interleukin (IL)-2 and IL-7 are cytokines that play crucial roles in the antitumor response by enhancing the survival, proliferation, differentiation, and function of immune cells. Modified forms such as human IL (hIL)-2/TCB2c and recombinant hIL (rhIL)-7-hyFc have demonstrated great promise in expanding populations of tumor-specific CD8⁺ T cells and improving the efficacy of cancer immunotherapy.

WHAT THIS STUDY ADDS

⇒ Our study shows that a combination of rhIL-7-hyFc and hIL-2/TCB2c synergistically suppresses tumor growth in mouse models of colon cancer. We further unveiled that these two cytokine-based therapies have discriminative but complementary roles in shaping and controlling antitumor CD8 responses. rhIL-7-hyFc significantly increases tumor-infiltrating CD62L⁺Ly108⁺ early progenitor exhausted T cell (T_{PEX}) cells and induces their differentiation into an intermediate exhausted subset of CD8⁺ T cells. In addition, rhIL-7-hyFc has the potential to counteract T-cell exhaustion. Conversely, hIL-2/TCB2c induces terminal differentiation into PD-1⁺TIM3⁺CD8⁺ T cells which are more likely to have cytolytic activity. Thus, these two cytokine-based therapies have distinct roles in the dynamics of antitumor CD8 T cells and their synergistic activity unveils a novel combination of cancer immunotherapy that could enhance the clinical efficacy of current checkpoint inhibitor treatments.

HOW THIS STUDY MIGHT AFFECT RESEARCH, PRACTICE OR POLICY

⇒ The findings suggest that rhIL-7-hyFc could be a mainstay modality for expanding tumor-infiltrating T_{PEX} cells, thereby improving the efficacy of both IL-2 and anti-PD-(L)1 cancer immunotherapy.

Moreover, rhIL-7-hyFc and hIL-2/TCB2c can overcome the limited therapeutic effectiveness of PD-1 blockade, culminating in the complete regression of tumors.

Conclusions rhIL-7-hyFc can expand and maintain the progenitor pool of exhausted CD8⁺ T cells, whereas hIL-2/

TCB2c promotes their differentiation into $T_{Ex\ term}$. Together, this induces an immune-stimulatory TME that improves the efficacy of checkpoint blockade.

INTRODUCTION

Interleukin (IL)-2 (aldesleukin) was the first cancer immunotherapy drug to be approved by the US Food and Drug Administration for metastatic renal cell carcinoma and melanoma. However, the use of high-dose aldesleukin is restricted due to the occurrence of capillary leak syndrome, the expansion of regulatory T cells (Tregs), and a poor pharmacokinetic profile.¹ To extend the half-life of IL-2, engineering approaches have been employed, including Fc fusion and PEGylation techniques.^{2,3} As a strategy to deliver IL-2 signaling selectively to CD8⁺ T cells and natural killer (NK) cells expressing low-affinity dimeric IL-2R β and IL-2R γ , mutant variants of IL-2 or IL-2/anti-IL-2 antibody immune complexes have been developed.⁴⁻⁶ The IL-2/anti-human IL (hIL)-2 antibody complex, hIL-2/TCB2c (SLC-3010), has been generated via complexing IL-2 with novel anti-human IL-2 antibody clone TCB2, which binds to the central part of CD25-binding interface on IL-2. hIL-2/TCB2c can preferentially stimulate CD122^{high} CD8⁺ T cells and NK cells, over Treg activation. Previous research has shown that this complex significantly inhibited the growth of murine melanoma and colon carcinoma, demonstrating further synergy with anti-CTLA-4 or anti-PD-1 antibodies.⁷ Currently, this complex is being investigated in phase I/ II clinical trials for patients with advanced solid tumors (NCT05525247).

IL-7 is a homeostatic, non-redundant, cytokine that plays a key role in the development, survival and proliferation of T cells, as well as maintenance of memory T cells. The potential antitumor effects of IL-7 have been evaluated with cancer vaccines, where it enhances the expansion and activation of vaccine-induced CD8⁺ T cells during tumor challenge. Consequently, this results in long-term protection and prolonged survival against cancer.⁸⁻¹¹ To overcome the major drawbacks of recombinant IL-7 and improve the in vivo half-life, we developed a long-acting recombinant human IL-7 (rhIL-7-hyFc, efineptakin alfa), comprising two IL-7 molecules fused to IgD/IgG4 elements. rhIL-7-hyFc is currently being investigated in multiple clinical trials both as a monotherapy and in combination with checkpoint inhibitors or cancer vaccines. Preclinical studies with rhIL-7-hyFc have shown that rhIL-7-hyFc enhances the antitumor efficacy of several anticancer strategies, including chemotherapy, radiotherapy, checkpoint inhibitors and adoptive cell therapies in murine tumor models.¹²⁻¹⁵

In this work, we sought to explore the synergistic efficacy and complementary mechanisms achieved through a dual combination therapy using rhIL-7-hyFc and hIL-2/TCB2c. A comprehensive understanding of the distinct functions of rhIL-7-hyFc and hIL-2/TCB2c is essential for the design of effective immunotherapeutic strategies

and for fully harnessing the immune system's potential in combating cancer.

RESULTS

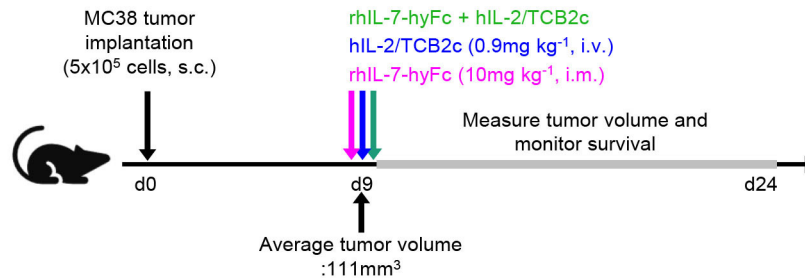
Combined treatment of rhIL-7-hyFc and hIL-2/TCB2c synergistically inhibits the growth of MC38 tumors

Given previous reports of antitumor effects with monotherapy of either rhIL-7-hyFc or hIL-2/TCB2c, we sought to evaluate the synergistic efficacy of combination therapy with rhIL-7-hyFc and hIL-2/TCB2c in the MC38 tumor model. Previous studies had shown antitumor activity of rhIL-7-hyFc at dose levels ranging from 1.25 mg/kg to 10 mg/kg and a single 10 mg/kg dose displayed antitumor activity in three different tumor models (MC38, CT-26, and TC-1).^{7,14} Given the results of dose-finding studies in the preclinical model (data not shown), 10 mg/kg of rhIL-7-hyFc was selected and used to explore the synergistic benefits with 0.9 mg/kg of hIL-2/TCB2c, which has shown some efficacy as a monotherapy. To evaluate the potential synergy of the combination therapy, MC38 tumor-bearing mice were injected with 10 mg/kg rhIL-7-hyFc and 0.9 mg/kg hIL-2/TCB2c via intramuscular and intravenous injection, respectively (figure 1A). As expected, both rhIL-7-hyFc and hIL-2/TCB2c monotherapies each resulted in marked delays in tumor growth compared with the untreated group. The combination of rhIL-7-hyFc and hIL-2/TCB2c significantly inhibited the growth of MC38 tumors compared with non-treated or monotherapy (figure 1B). The tumor individual growth curves are presented in (figure 1C). Collectively, these results indicate that the combination of rhIL-7-hyFc and hIL-2/TCB2c enhanced antitumor efficacy.

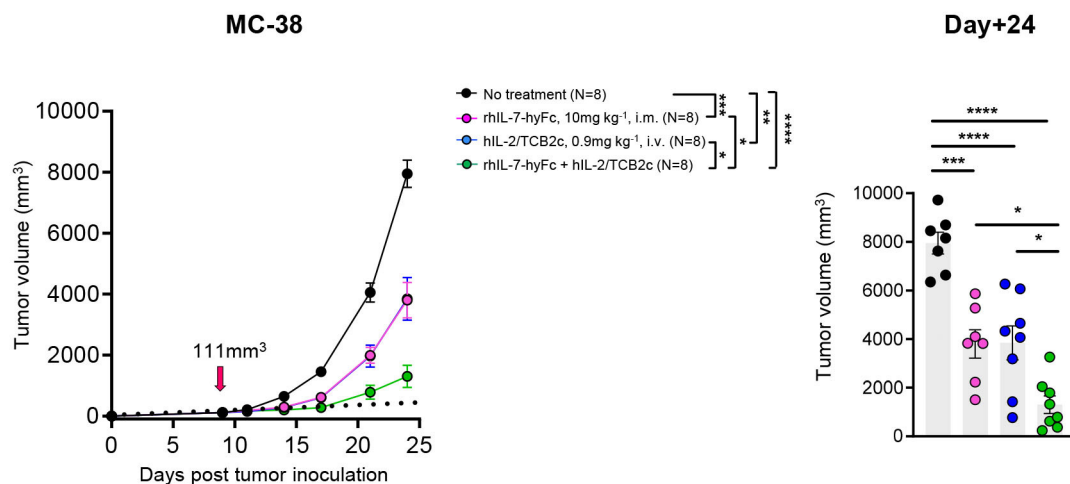
rhIL-7-hyFc generates an immune-stimulatory tumor microenvironment

To understand the underlying mechanism for the increased tumor growth suppression, we first analyzed the immune changes elicited by each one of the cytokines separately or in combination. CD8⁺ T-cell numbers and proportions from the tumor, tumor-draining lymph nodes (tdLN), and peripheral blood were analyzed on days 4, 7, and 10 post-treatment. Consistent with our previous findings, CD8⁺ T cells started to increase significantly after day 4 and reached peak levels at day 7 following rhIL-7-hyFc or hIL-2/TCB2c administration (figure 2A). We observed a decline in CD8⁺ tumor-infiltrating lymphocyte (TIL) numbers 10 days after treatment in all treatment groups, although mice treated with rhIL-7-hyFc, alone or in combination with hIL-2/TCB2c, maintained significantly higher CD8⁺ TIL than the non-treated and hIL-2/TCB2c-treated groups. When we further assessed the abundance of CD8⁺ T cells in the tdLN (figure 2A) and peripheral blood (online supplemental figure 1A), a massive expansion of CD8⁺ T cells was observed in the rhIL-7-hyFc monotherapy and combination therapy groups, which peaked around the same time as CD8⁺ TIL numbers. A single-dose injection of hIL-2/TCB2c also

A



B



C

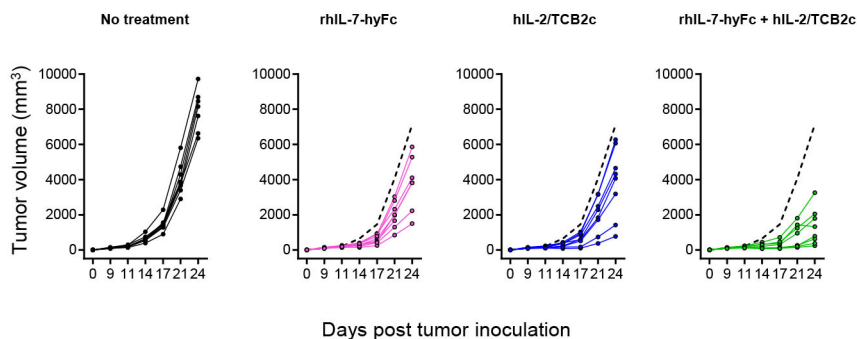


Figure 1 Combined treatment of rhIL-7-hyFc and hIL-2/TCB2c synergistically inhibits the growth of MC38 tumors. (A) Schematic overview of experimental design. MC38 tumor cells were injected subcutaneously at day 0 (d0). 10mg/kg rhIL-7-hyFc or 0.9mg/kg hIL-2/TCB2c was administered intramuscularly (i.m.) and intravenously (i.v.) on day 9 (d9). Tumor growth of MC38 tumors treated with the indicated therapies (n=8 per group) is shown as (B) average tumor size per treatment group; red arrow indicates treatment start; tumor volumes on day 24 post-implant are highlighted in a bar graph (C) individual tumor growth curves; the dashed line represents the average tumor volume of non-treated mice. Data are presented as the mean±SEM and analyzed by one-way (B; right panel) or two-way analysis of variance (B; left panel) with Turkey's testing for multiple comparisons. Statistical significance is indicated as *p<0.05, **p<0.01, ***p<0.001, ****p<0.0001. i.v., intravenously; rhIL, recombinant human interleukin; s.c., subcutaneous.

resulted in a modest expansion of CD8⁺ T cells in tdLNs, peaking on day 4 after administration, but the number of CD8⁺ T cells in the bloodstream did not change. These results confirm that the significant and persistent expansion of CD8⁺ T cells in tumor and peripheral organs is mainly mediated by rhIL-7-hyFc.

For a deeper understanding of alternations in the immune cell infiltration after therapy, we comprehensively analyzed the immune compartment of the TME, with a focus on CD8⁺ T cells, CD11b⁺ myeloid-derived suppressor cells (MDSCs), and Treg cells. rhIL-7-hyFc therapy resulted in a significant increase in the frequency

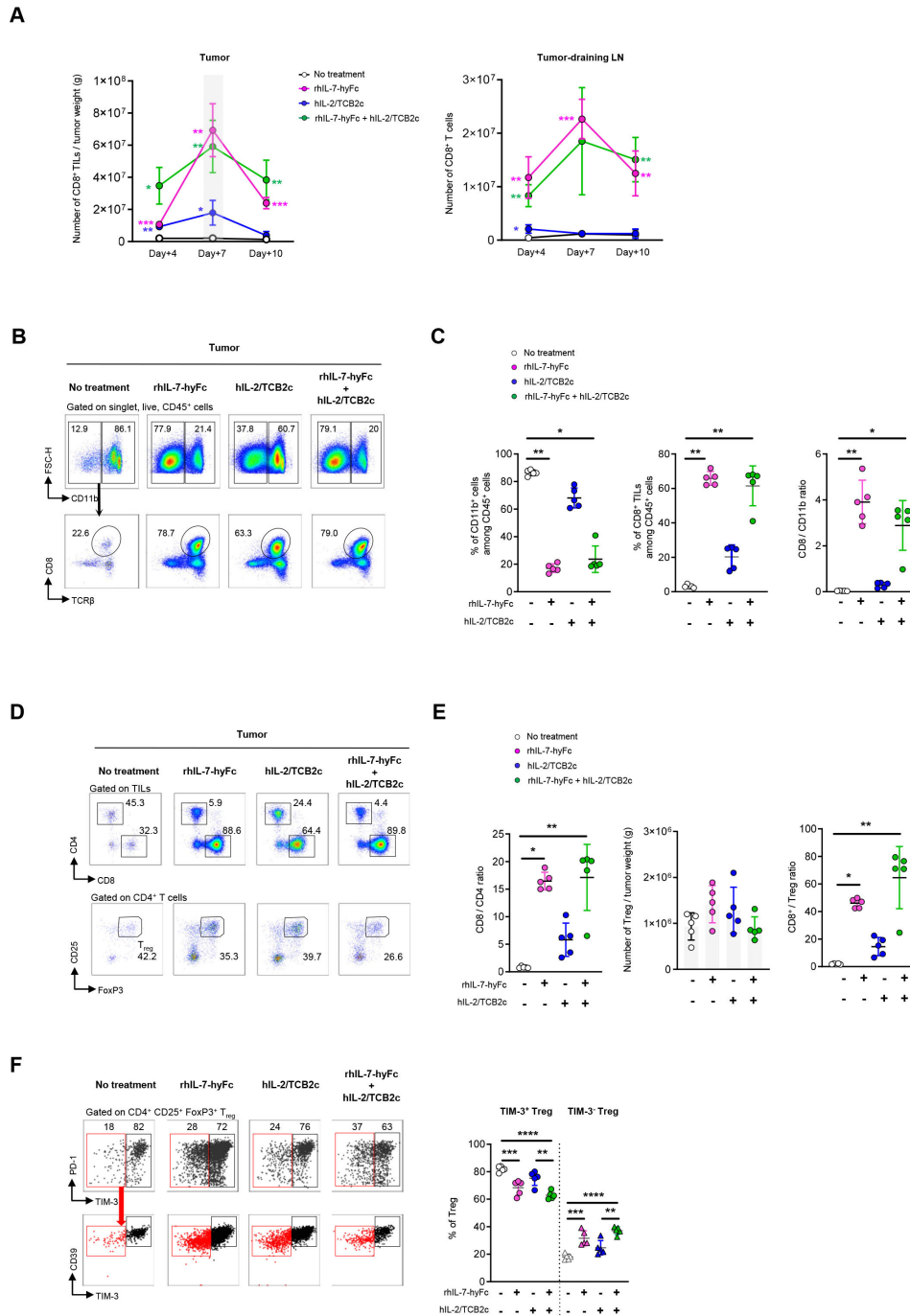


Figure 2 rhIL-7-hyFc generates immune-stimulatory tumor microenvironment. (A) Absolute counts of total CD8 T cells in the tumor (left panel) and tumor-draining lymph node (right panel) at 4, 7 and 10 days post-treatment. The asterisk (*) expresses significance compared with the non-treated control. (B) Representative flow cytometry plots showing the frequency of CD11b⁺ cells (upper panel) and TCRβ⁺ CD8⁺ T cells (lower panel) among CD45⁺ cells isolated from MC38 tumors on 7 days after the first dose and pooled data (right panel) showing the percentage of TCRβ⁺ CD8⁺ T cell among CD45⁺ tumor-infiltrating immune cells. (C) Summary graphs showing the percentage of CD11b⁺ cells (left), CD8⁺ cells (middle) in total tumor infiltrating CD45⁺ leukocytes, and CD8/CD11b ratio (right) at 7 days post-treatment. (D) Representative flow cytometry plots showing percentage of CD4 or CD8 T cells (upper panel), pre-gated on live, singlets, CD45⁺, CD11b⁻, TCRβ⁺ and CD25⁺FoxP3⁺Tregs (lower panel) gated on CD4 T cells from MC38 tumors 7 days post-treatment. (E) Pooled data showing CD8/CD4 ratios (left panel), CD4⁺CD25⁺FoxP3⁺ Treg cell number (middle panel) and CD8/Treg ratios (right panel) in tumor 7 days post-treatment. (F) Representative flow plots showing the percentage of two subpopulations of intratumoral Treg cells based on the expression of TIM-3 (upper panel). Red dots represent the TIM-3⁻ Tregs. Pooled data of the frequency of TIM-3⁺ and TIM-3⁻ Treg cells is shown in the right panel. All data are represented as mean±SD (n=5 mice per group). Statistical analysis was performed by using one-way analysis of variance with Tukey's multiple comparisons test. Statistical significance is indicated as *p<0.05, **p<0.01, ***p<0.001, ****p<0.0001. LN, lymph node; rhIL, recombinant human interleukin; TIL, tumor-infiltrating lymphocyte; TIM-3, T cell immunoglobulin and mucin domain-3; Treg, regulatory T cells.

of CD8⁺ TIL among CD45⁺ cells, while remarkably reducing the frequencies of CD11b⁺ MDSCs. This resulted in prominently enhanced ratios of CD8⁺ T cells relative to CD11b⁺ MDSC more obviously 7 days after treatment (figure 2B,C). On the other hand, hIL-2/TCB2c-treated tumors exhibited a modest increase in the frequency of CD8⁺ TILs among total CD45⁺ cells, due to slightly lower frequencies in CD11b⁺ MDSC than untreated mice. Altogether, our results corroborated that rhIL-7-hyFc therapy remodels the immune microenvironment via extensive infiltration of CD8⁺ TILs, further decreasing the proportion of CD11b⁺ MDSCs.

We next examined whether monotherapy or combination treatment leads to the expansion of Treg cells in the TME. On day 7 after rhIL-7-hyFc alone or combination treatment, markedly increased CD8/CD4 ratios were observed compared with those in the non-treated group while the total numbers of Treg cells were not significantly different between groups. rhIL-7-hyFc-containing treatment favored a much higher ratio of CD8/Treg when compared with the untreated group (figure 2D,E). Furthermore, it is known that TIM-3⁺ Tregs have enhanced immunosuppressive activity and are associated with worse prognosis.^{16,17} Interestingly, rhIL-7-hyFc effectively reduced the proportion of TIM-3⁺ Treg cells within the tumor, inversely increasing TIM-3⁻ Treg cells characterized by having low expression of CD39, compared with those from untreated mice (figure 2F). Taken together, these findings suggest that rhIL-7-hyFc established an immune-stimulatory microenvironment characterized by intensive infiltration of cytotoxic CD8⁺ T cells, and lower frequency of immunosuppressive cells like TIM-3⁺ Tregs and CD11b⁺ MDSCs.

Combination therapy of rhIL-7-hyFc and hIL-2/TCB2c can greatly expand both tumor-specific and non-specific CD8⁺ T cells in tumors

The combination of rhIL-7-hyFc and hIL-2/TCB2c resulted in a synergistic increase in the absolute number of CD44^{high}PD-1⁺CD8⁺ T cells in the TME (figure 3A). We next investigated the tumor specificity of the CD8⁺ TILs in MC38 tumors treated with monotherapy or combination therapy. Three major subpopulations of CD8⁺ TIL were described based on PD-1 expression and binding to the MC38 epitope peptide (p15E₆₀₄₋₆₁₁, KSPWF^TTLL), enabling the identification of endogenous p15E-specific CD8⁺ T cells (figure 3B).¹⁸ CD8⁺ TILs were classified into three discernible subpopulations: PD-1⁻p15E⁻, PD-1⁺p15E⁻, and PD-1⁺p15E⁺ (tumor-specific and reactive).

We hypothesized that combination treatment exerts antitumor activity by the differential effects of rhIL-7-hyFc and hIL-2/TCB2c on CD8⁺ TIL subsets. Previous studies have shown that engineered IL-2 variants with attenuated binding to CD25 and increased affinity for CD122 can induce tumor-specific T-cell responses along with cytotoxic T-cell expansion in preclinical models.^{19,20} Consistent with this, hIL-2/TCB2c markedly increases the frequency of p15E-specific CD8⁺ T cells, but does not lead

to alternations in their absolute numbers compared with the untreated control (figure 3C). On the other hand, rhIL-7-hyFc preferentially increases the proportion of PD-1⁻p15E⁻, while the frequency of p15E-specific CD8⁺ T cells remains comparable to that of the non-treated group. However, due to a significant increase in absolute counts of CD8⁺ TIL driven by rhIL-7-hyFc compared with hIL-2/TCB2c as shown in figure 2A, and a marginal increase is observed in the counts of p15E-specific CD8⁺ T cells (figure 3C). It is important to note that no statistical difference is found between the non-treated and rhIL-7-hyFc-treated group. Interestingly, the combination of rhIL-7-hyFc plus hIL-2/TCB2c significantly increases the counts of p15E-specific CD8⁺ T cells. The complementary effect of single agents contributes to augmenting the count of p15E-specific CD8⁺ T cells. While rhIL-7-hyFc leads to an increase in the number of tumor-infiltrating CD8⁺ T cells, hIL-2/TCB2c has the effect of elevating the percentage of p15E⁺ cells within the subsets of CD8⁺ TIL. Additionally, this combination also effectively enhances the counts of PD-1⁻p15E⁻ and PD-1⁺p15E⁻ CD8⁺ T cells inside the tumor. In conclusion, the combination therapy leads to simultaneous increases in the numbers of both intratumoral PD-1⁻CD8⁺ and PD-1⁺CD8⁺ T cells.

rhIL-7-hyFc selectively expands CD62L⁺Ly108⁺ progenitor of exhausted CD8⁺ cells

To gain further insights into whether and how dual combination therapy affects the phenotypic heterogeneity of exhausted CD8⁺ T cells in the tumor and peripheral blood, we examined PD-1⁺CD8⁺ T-cell responses at two different time points (4 and 7 days post-treatment). Consistent with multiple reports, we observed that PD-1⁺CD8⁺ T cells included two distinct populations that expressed either TCF-1 or TIM-3 (figure 4A), which are prominent markers to distinguish precursor exhausted cells (TCF-1⁺TIM-3⁻, progenitor exhausted T cell (T_{PEX})) and terminally exhausted cells (TCF-1⁻TIM-3⁺, terminally exhausted T cell (T_{EX term})).²¹⁻²³ When comparing the treatments, differential effects were seen on the exhausted CD8⁺ T-cell subsets. At 4 days post-treatment, rhIL-7-hyFc significantly increases both the percentage and absolute counts of CD62L⁺Ly108⁺ T_{PEX} cells which possess a stem-like capacity such as high self-renewal ability and multipotency.²⁴ Most importantly, this effect is observed in both PD-1⁺CD44^{high} (figure 4A,B) and p15E-specific CD8⁺ T cells in tumors (figure 4C,D). Notably, CD62L⁺Ly108⁺ T_{PEX} was distinguished from naïve and memory CD8⁺ T cells in terms of PD-1 and TOX expression (online supplemental figure 2A). Additionally, at 7 days after rhIL-7-hyFc treatment, the increased fraction of CD62L⁺Ly108⁺ T_{PEX} cells was stably maintained in the blood (figure 4E,F).

At day 7 post rhIL-7-hyFc treatment, the frequency of tumor-infiltrating CD62L⁺Ly108⁺ T_{PEX} cells displayed no significant difference from non-treated control. However, the absolute number of CD62L⁺Ly108⁺ T_{PEX} cells was still significantly higher in the rhIL-7-hyFc-treated mice

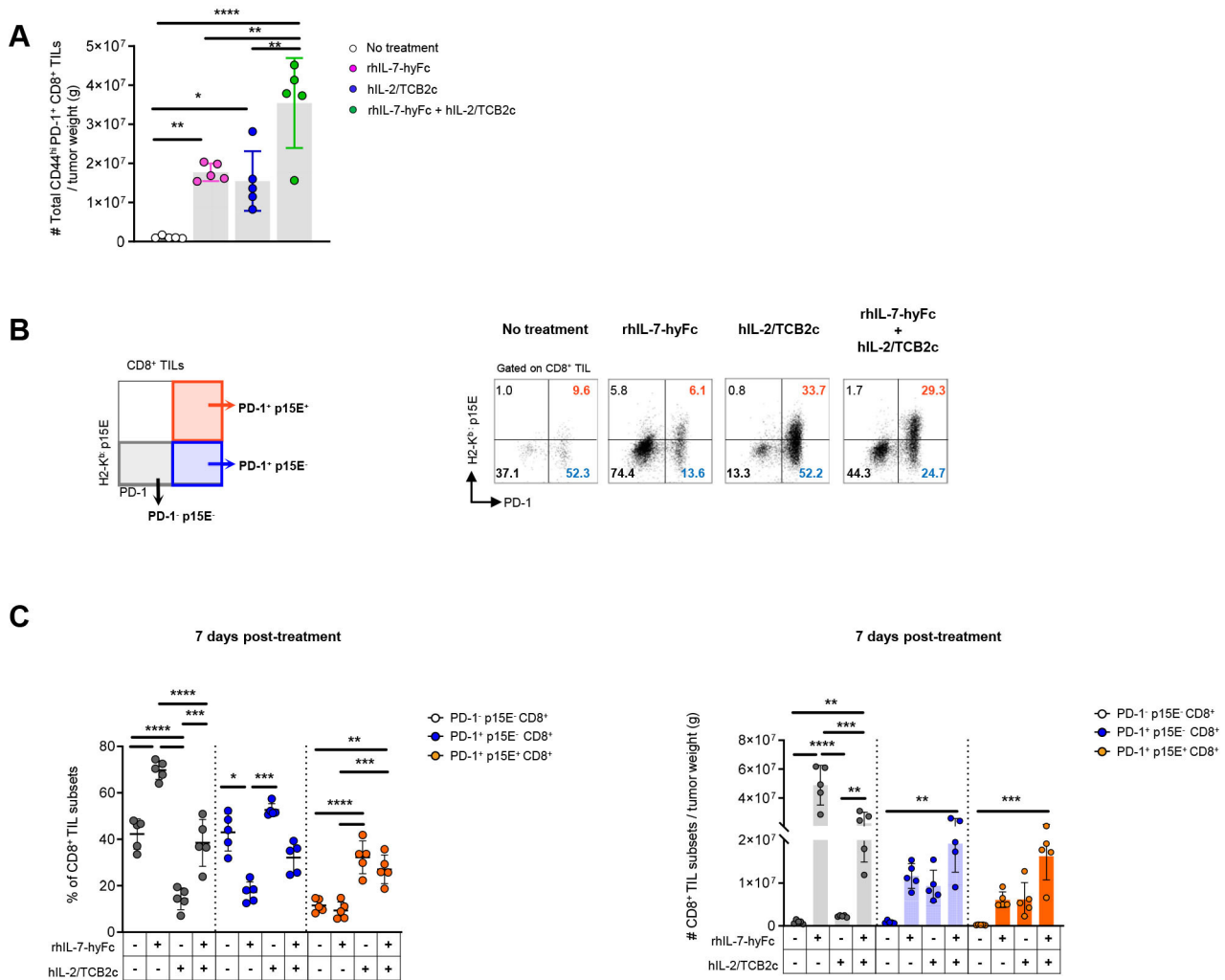


Figure 3 Combination therapy of rhIL-7-hyFc and hIL-2/TCB2c increases both tumor-specific and non-specific CD8⁺ T cells in the tumor microenvironment. (A) Absolute numbers of CD44^{high}PD-1⁺CD8⁺ T cells in MC38 tumors. (B) Left panel shows gating strategy for phenotypic analysis of three subsets (PD-1⁻p15E⁻, PD-1⁺p15E⁻, and PD-1⁺p15E⁺) of intratumoral CD8⁺ T cells and representative flow cytometry plots of PD-1 and p15E MHC class I H-2K^b Dextramer staining against MC38 tumors are shown in the right panel. (C) Pooled data showing percentages (left panel) and absolute numbers (right panel) of three subsets of CD8⁺ T cells in MC38 tumors. PD-1⁻p15E⁻CD8⁺ TILs are depicted in gray; PD-1⁺p15E⁻ in blue; PD-1⁺p15E⁺ in orange. Tumor-infiltrating CD8⁺ T cells were isolated and analyzed on 7 days post-treatment. All intratumoral absolute numbers were normalized to tumor weight. Data are presented as mean±SD (n=5 per group). *p<0.05; **p<0.01; ***p<0.001, ****p<0.0001 by one-way analysis of variance followed by Tukey's multiple comparisons test in (A, C–D). MHC, major histocompatibility complex; PD-1, programmed cell death protein 1; rhIL, recombinant human interleukin; TIL, tumor-infiltrating lymphocyte.

than in any other group (online supplemental figure 2B and C). We hypothesized that CD62L⁺Ly108⁺ T_{PEX} cells, which were present at higher frequency 4 days after rhIL-7-hyFc injection, could differentiate into an intermediate exhausted population under persistent antigen exposure. To better characterize intermediate exhausted CD8 T cells (T_{EX int}), we validated eight markers in mice for identifying these cells within a continuum process of exhaustion: CD62L, Ly108, PD-1, CD39, CD25, CD44, granzyme B, and CD69 (figure 5). We compared protein expression profiles between TCF-1⁺TIM-3⁻, TCF-1⁻TIM-3⁻, and TCF-1⁻TIM-3⁺ cells among PD-1⁺CD8⁺ TILs from untreated mice. Based on the intermediate expression levels of PD-1, CD39, CD25, CD44, and granzyme B, we considered PD-1⁺ TCF-1⁻TIM-3⁻ population as T_{EX int}.

We next profiled the response of PD-1⁺CD8⁺ TILs to monotherapy and combination therapy at 7 days post-treatment. Strikingly, in rhIL-7-hyFc-treated tumors, the frequencies of T_{PEX} and T_{EX int} were increased by 3.9-fold and 2.3-fold higher compared with those of the hIL-2/TCB2c-treated group (figure 7B,C). More importantly, this increase coincided with a marked increase in absolute numbers of T_{PEX} and T_{EX int} (figure 7C). Conversely, after hIL-2/TCB2c treatment, the proportion of T_{EX term} was substantially increased, followed by the drastic reduction in the frequency of T_{PEX}, consistent with that seen 4 days post-treatment. This suggests that hIL-2/TCB2c treatment favors the terminal differentiation of T_{PEX} cells. When hIL-2/TCB2c was administered in combination with rhIL-7-hyFc, this combination strategy can

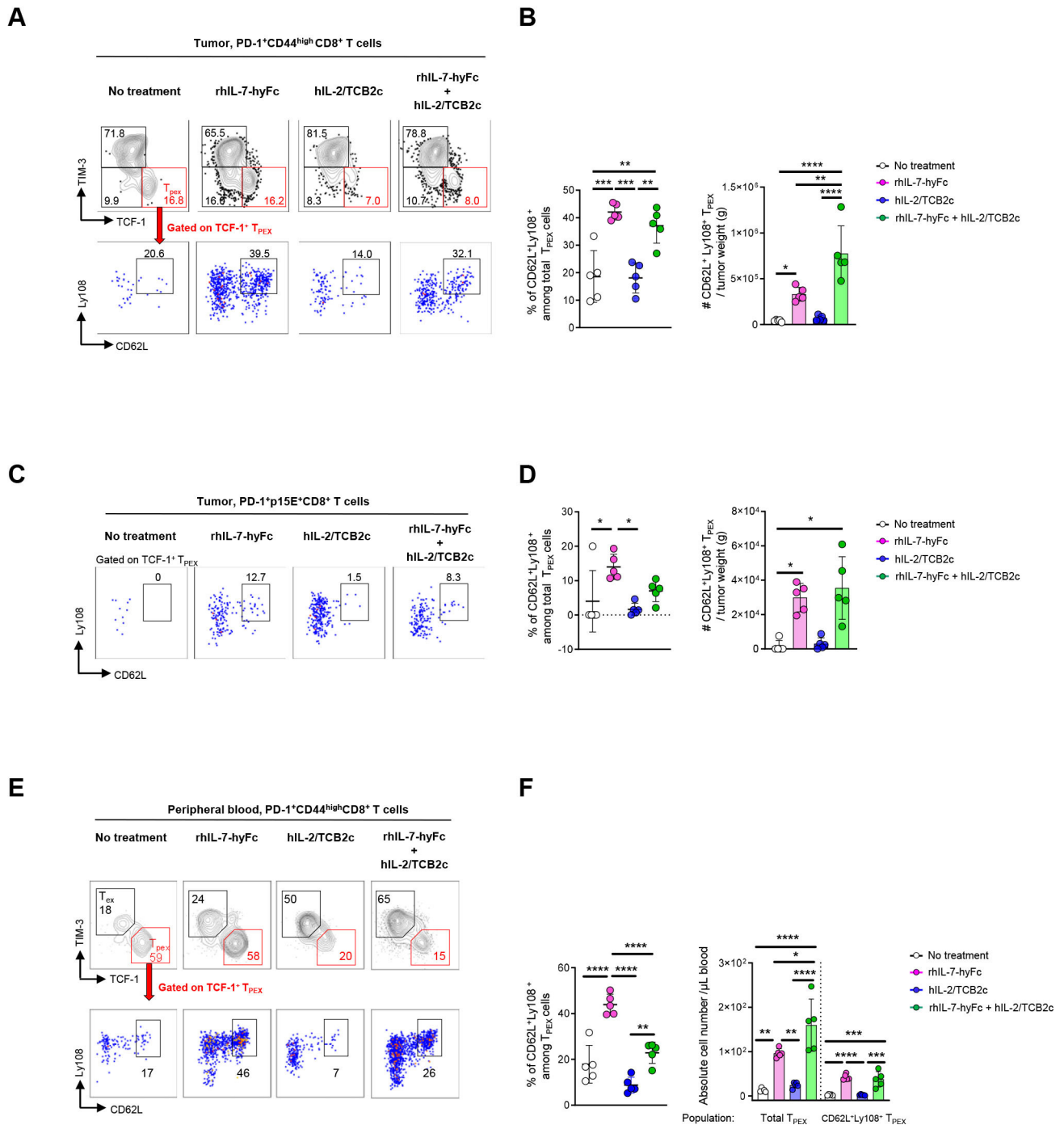


Figure 4 rhIL-7-hyFc selectively expands CD62L⁺Ly108⁺ early progenitor of exhausted CD8⁺ T cells. (A) Representative flow cytometry plots showing the gating strategy used to identify CD62L⁺Ly108⁺ T_{PEX} among PD-1⁺CD44^{high}CD8⁺ T cells on 4 days post-treatment. (B) Pooled data showing the frequencies (left panel) and absolute numbers (right panel) of CD62L⁺Ly108⁺ T_{PEX}. (C) Representative flow cytometry plots of CD62L⁺Ly108⁺ T_{PEX} among PD-1⁺p15E⁺CD8⁺ T cells after 4 days post-treatment. (D) Percentages (left panel) and absolute numbers (right panel) of CD62L⁺Ly108⁺ T_{PEX}. (E) Representative flow cytometry analysis of CD62L⁺Ly108⁺ T_{PEX} among PD-1⁺CD44^{high}CD8⁺ T cells in peripheral blood of MC38 tumor-bearing mice at 7 days post-treatment. (F) Frequency (left panel) and absolute numbers (right panel) of CD62L⁺Ly108⁺ T_{PEX} in peripheral blood from MC38-bearing mice. Absolute numbers were normalized to tumor weight or volume of blood as indicated. The data are represented as the mean ± SD, n=5 per group. *p<0.05; **p<0.01; ***p<0.001 and ****p<0.0001 by one-way analysis of variance with Tukey's multiple comparison test. PD-1, programmed cell death protein 1; rhIL, recombinant human interleukin; TCF-1, T cell factor 1; TIM-3, T cell immunoglobulin and mucin domain-3; T_{PEX}, progenitor exhausted T cell.

prevent severe CD8⁺ T-cell exhaustion, leading to an increase in the numbers of T_{PEX} compared with those from mice treated with hIL-2/TCB2c alone. Likewise,

we found that phenotypic changes of p15E-specific CD8⁺ TIL after treatments were consistent with that observed in PD-1⁺CD44^{high}CD8⁺ T cells as aforementioned (online

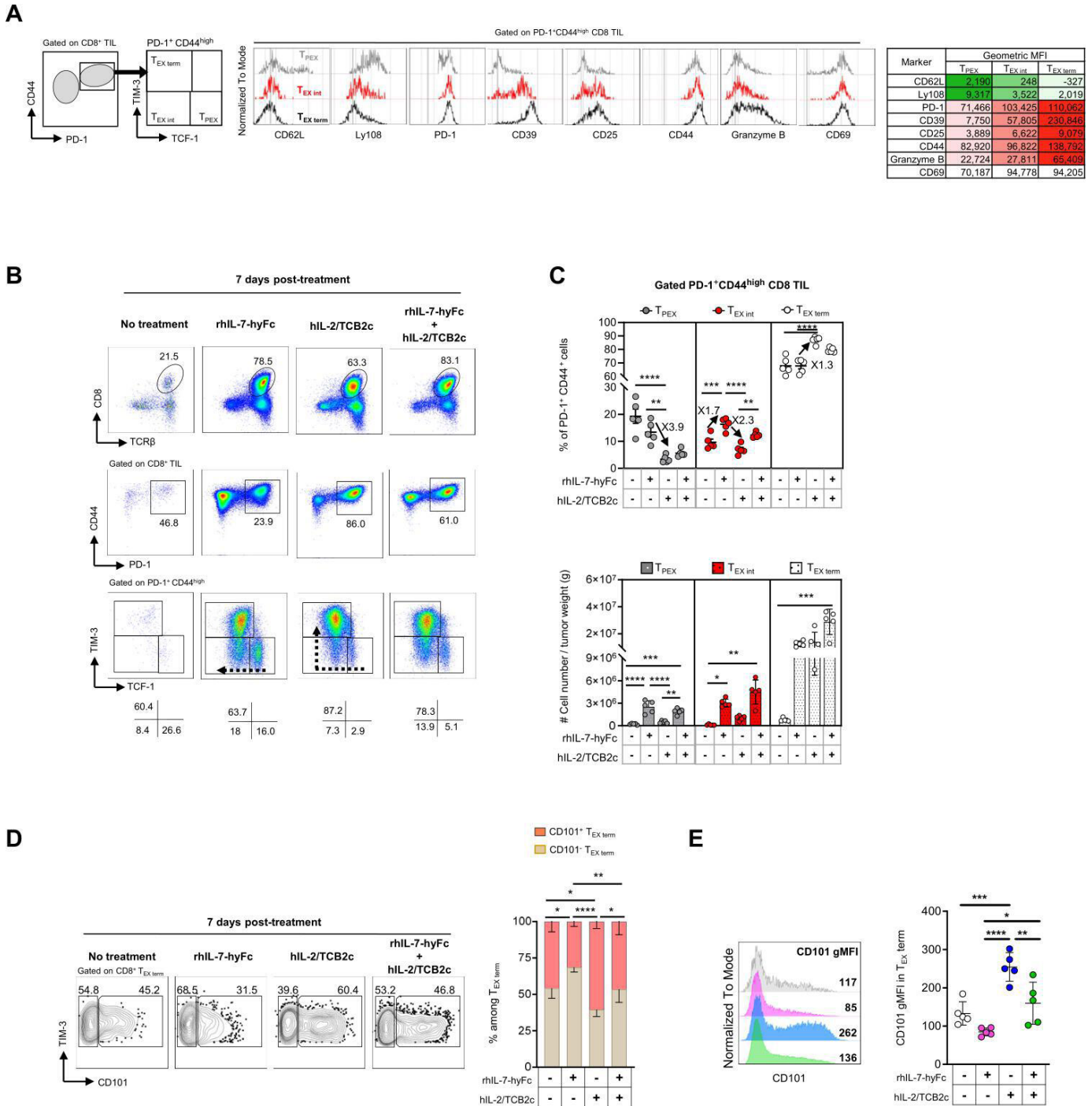


Figure 5 rhIL-7-hyFc sustains T_{PEX} cells in the tumor, and hIL-2/TCB2c differentiates T_{PEX} cells into terminally differentiated cells (T_{EX term}). (A) Representative histograms (left panel) showing the expression of activation (CD25, CD44, CD69), exhaustion (PD-1, CD39), progenitor (Ly108 [also known as SLAMF6], CD62L), and cytotoxicity (Granzyme B) markers on TCF-1⁺TIM-3⁺ (T_{PEX}), TCF-1⁺TIM-3⁻ (T_{EX int}), and TCF-1⁻TIM-3⁺ (T_{EX term}) cells among PD-1⁺CD44^{high}CD8⁺ TILs from untreated mice. Geometric mean fluorescence intensity (gMFI) on each subset is shown in the right panel. (B) Representative flow cytometry plots and (C) summary graphs showing the frequencies (top panel) and absolute numbers (bottom panel) of T_{PEX}, T_{EX int}, T_{EX term} among all PD-1⁺CD44^{high}CD8⁺ TILs from MC38 tumors from different treatment groups (D) Representative flow cytometry plots (left panel) showing CD101 and TIM-3 expression on CD8⁺ T_{EX term}. Pooled data (right panel) shows the percentage of CD101⁺ and CD101⁺ on CD8⁺ T_{EX term}. (E) Representative histogram (left panel) depicting CD101 expression on CD8⁺ T_{EX term} in MC38 tumors from non-treated (grey) and rhIL-7-hyFc (magenta), hIL-2/TCB2c (blue), and rhIL-7-hyFc plus hIL-2/TCB2c (green) treated mice. Summary data (right panel) shows the geometric MFI of CD101 on each treatment group. Phenotypic analysis of CD8⁺ TILs was performed 7 days post-treatment. Intratumoral absolute numbers were normalized to tumor. Each treatment group consisted of 5 mice, showing mean ± SD. Statistical significance is indicated as *p<0.05, **p<0.01, ***p<0.001, ****p<0.0001. T_{PEX}, progenitor exhausted T cell; T_{EX int}, intermediate exhausted T cell; T_{EX term}, terminally exhausted T cell.

supplemental figure 3A and B). Together, these data demonstrate that rhIL-7-hyFc enables T_{PEX} cells to retain a less-differentiated state, whereas hIL-2/TCB2c can progressively convert T_{PEX} cells into $T_{EX\ term}$ throughout tumor development.

Collectively, we have shown persuasive evidence that combination therapy can confer synergistic tumor control through two main mechanisms—increased abundance of T_{PEX} cells and subsequently their rapid differentiation into functional effector T cells by rhIL-7-hyFc and hIL-2/TCB2c treatment, respectively.

rhIL-7-hyFc and hIL-2/TCB2c have differential effects on the phenotype of terminally exhausted $CD8^+$ TILs

To further delineate the phenotypes of $T_{EX\ term}$ cells after single and combination therapy, we analyzed CD101 expression on $T_{EX\ term}$ cells to discriminate $CD101^-$ TIM-3⁺ and $CD101^+$ TIM-3⁺ subsets. Recent studies have shown that $CD101^-$ TIM-3⁺ cells have superior cytolytic activity in a chronic viral model and they irreversibly convert into fully exhausted $CD101^+$ TIM-3⁺ $CD8^+$ T cells, which is characterized by a loss of proliferative potential, upregulated inhibitory receptors, and impaired cytokine production.^{25,26} Here, we demonstrated that the majority of the $T_{EX\ term}$ population in the rhIL-7-hyFc-treated tumor were $CD101^-$ cells. In contrast, most of the $CD8^+$ $T_{EX\ term}$ isolated from the hIL-2/TCB2c-treated group are $CD101^+$ cells, with increased CD101 expression intensity (figure 7F,G). Altogether, these findings indicated that rhIL-7-hyFc induces a functional intermediate state of exhaustion, whereas hIL-2/TCB2c favors differentiation into more terminally differentiated $CD8^+$ T cells. Altogether, these findings suggest that rhIL-7-hyFc favors the maintenance of a less-differentiated progenitor pool to support the progressive differentiation induced by hIL-2/TCB2c.

rhIL-7-hyFc induces robust proliferation of T_{PEX} cells in the tumor-draining lymph node

Our data showed enlarged tdLN and increased cellularity starting at day 4 and peaking at day 7 after rhIL-7-hyFc treatment, while hIL-2/TBC2c did not show any increase in size and cellularity (figure 8A). The onset of enlarged tdLN, typically beginning around day 4 after rhIL-7-hyFc treatment, overlaps with the time point where we observed a significant increase in the percentage of intratumoral $CD62L^+Ly108^+$ T_{PEX} . Based on these findings, we hypothesized that rhIL-7-hyFc could lead to extensive proliferation of T_{PEX} cells in tdLN, thereby resulting in higher proportions and numbers of $CD62L^+Ly108^+$ T_{PEX} in the tumor. To test this possibility, we examined the frequency of proliferating Ki-67⁺ T_{PEX} cells within the tdLN at day 7 after treatment. rhIL-7-hyFc potently increases the frequency and the number of proliferating T_{PEX} cells rather than hIL-2/TCB2c (figure 8B,C). Additionally, T_{PEX} cells in rhIL-7-hyFc-treated tdLN are more actively cycling, as demonstrated by increased expression of Ki-67, when compared with those in hIL-2/TCB2c-treated animals (figure 8D). Thus, our data corroborated

that rhIL-7-hyFc induces extensive proliferation of T_{PEX} in tdLN and sustains more functional T_{PEX} cells in terms of proliferation capacity than hIL-2/TCB2-treated mice. These data implicate that rhIL-7-hyFc can provide a supportive niche enriched for T_{PEX} cells with high proliferation capacity in tdLNs.

Moreover, we explored the reliance of rhIL-7-hyFc-induced $CD8^+$ T-cell response in tdLN on the antitumor immune responses using FTY720. The results indicate that administration of FTY720 before tumor inoculation promotes tumor growth and progression in mice treated with rhIL-7-hyFc, either alone or in combination with hIL-2/TCB2c, implying the significance of $CD8^+$ T-cell responses in tdLN after rhIL-7-hyFc-containing combination treatments. In conclusion, our findings highlight the critical role of $CD8^+$ T-cell responses within the tdLN for the effective antitumor efficacy of the dual combination treatment (data not shown).

rhIL-7-hyFc and hIL-2/TCB2c improves the antitumor efficacy of PD-1 blockade therapy

We previously have shown that the combination of rhIL-7-hyFc plus hIL-2/TCB2c more effectively inhibited tumor growth than single modality treatments, but it did not lead to complete tumor clearance in mice. Based on the above findings, we hypothesized that the addition of an anti-PD-1 inhibitor to rhIL-7-hyFc and hIL-2/TCB2c elicits synergistic antitumor effects, driven by the induction of a proliferative burst in $CD8^+$ T_{PEX} cells.

Next, we compared antitumor therapeutic effects induced by dual (rhIL-7-hyFc plus hIL-2/TCB2c) and triple combination (rhIL-7-hyFc plus hIL-2/TCB2c plus anti-PD-1 inhibitor) treatment in two syngeneic colon cancer models, MC38 and CT26. In the MC38 tumors, the triple combination therapy inhibited tumor growth more effectively than the dual-agent combination and five animals out of nine (55%) were rendered completely tumor-free at day 28, while no complete tumor regression was observed in the dual-agent combination group (figure 7). In comparison to MC38 models, the difference in tumor growth rate between double and triple combination in the CT26 tumor model did not reach statistical significance (figure 7). However, the triple combination induced eradication of established CT26 tumors in seven out of eight (87% tumor-free) mice after 18 days following initial treatment, whereas none of the mice in the dual combination group showed complete regression (figure 7). Ultimately, PD-1 signaling blockade increased the rate of complete tumor regression when administered together with rhIL-7-hyFc and hIL-2/TCB2c. Collectively, these results show that through differential effects on exhausted $CD8^+$ T-cell subsets, rhIL-7-hyFc and hIL-2/TCB2c combination can synergize with PD-1 blockade to significantly improve therapeutic efficacy. Moreover, in mice treated with the triple combination, no observable adverse responses, such as body weight loss or elevated levels of aspartate aminotransferase (AST), alanine aminotransferase (ALT), alkaline phosphatase

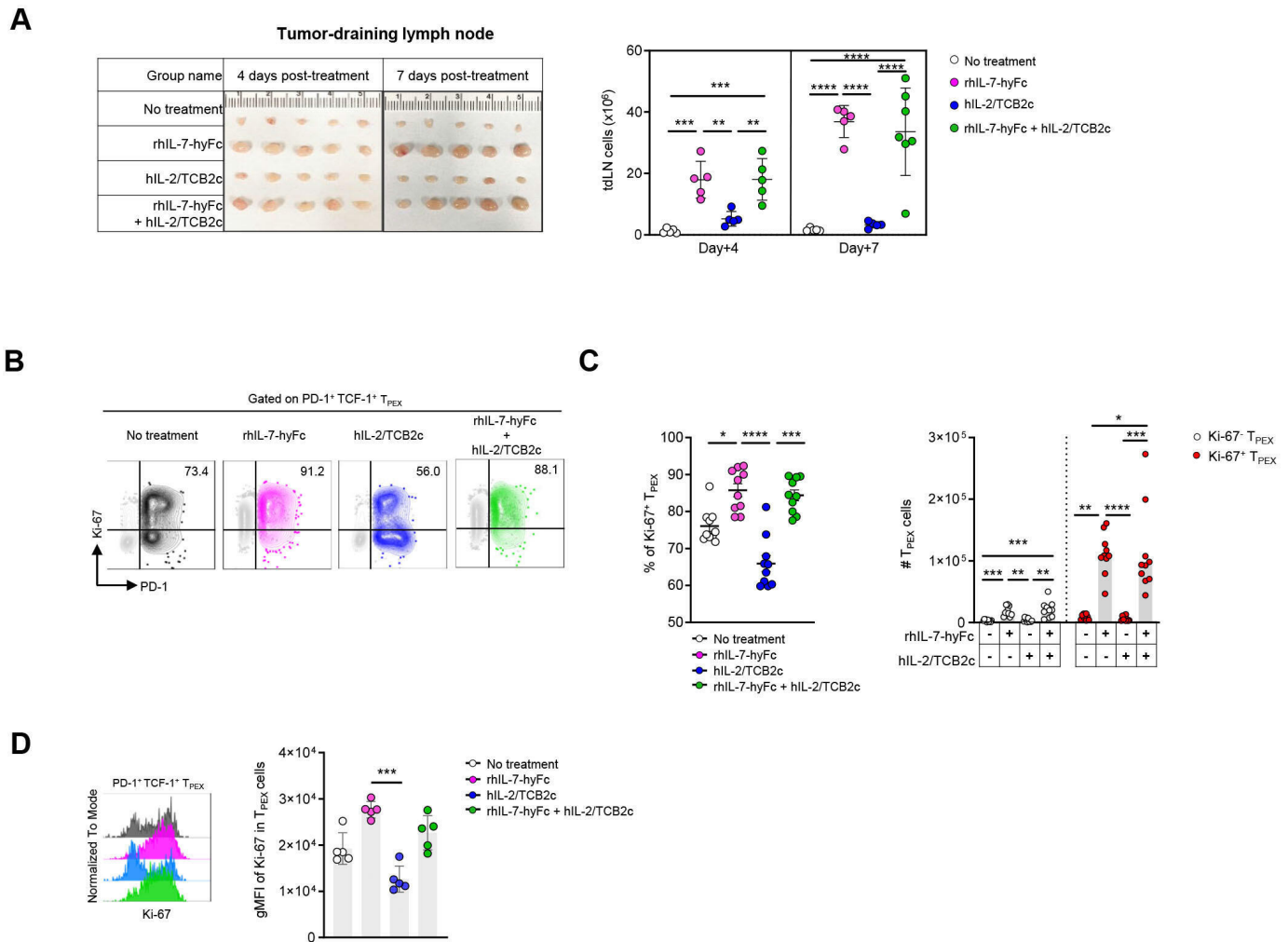


Figure 6 rhIL-7-hyFc induces robust proliferation of T_{PEX} cells in tumor-draining lymph node. (A) Sizes (left panel) and cellularity (right panel) of tumor-draining lymph nodes (tdLN, inguinal) from MC38 tumor-bearing mice at the indicated time points (4 and 7 days post-treatment). (B) Representative contour plots showing Ki-67⁺ T_{PEX} cells overlaid on total CD8⁺ T cells in tdLN on 7 days post-treatment. (C) Frequencies (left panel) and absolute numbers (right panel) of Ki-67⁺ T_{PEX} among total CD8⁺ T_{PEX} cells in tdLNs. (D) Representative histogram (left panel) and pooled data (right panel) of geometric mean fluorescence intensity (gMFI) of Ki-67 in T_{PEX} cells in tdLNs. In graphs, each dot represents an individual mouse. Data are expressed as mean±SD (A, D) or mean±SEM (C) and analyzed by one-way analysis of variance with Tukey's multiple comparisons test. Statistical significance is indicated as **p*<0.05, ***p*<0.01, ****p*<0.001, *****p*<0.0001. PD-1, programmed cell death protein 1; rhIL, recombinant human interleukin; TCF-1, T cell factor 1; T_{PEX}, progenitor exhausted T cell.

(ALP), IL-6, and IL-1 β , were detected (data not shown). The findings of this investigation have enabled the proposition of a novel triple combination strategy to enhance the therapeutic effects of cancer immunotherapy.

DISCUSSION

Recent studies have identified the presence of exhausted CD8⁺ T cells expressing TCF-1, which are considered T_{PEX} cells, in both chronic viral infection and cancer.^{26–28} In patients with cancer, the presence of TCF-1^{high}PD-1⁺ CD8 TILs shows promise as a potential predictive biomarker for the response to anti-PD-(L)1 therapy. In patients with non-small cell lung cancer, an increasing number of TCF-1⁺PD-1⁺ TILs have been observed to be positively correlated with improved survival outcomes in response

to anti-PD-1 therapy.²⁹ Similarly, in patients with metastatic melanoma, an enhanced frequency of TCF7⁺CD8⁺ T cells in tumors has been associated with better survival and response to immune checkpoint inhibitor (ICI) therapy.³⁰ Additionally, mechanistic studies have highlighted T_{PEX} as the major subset that responds to checkpoint blockade.^{21,31} Thus, T_{PEX} cells represent an important target cell, that is, associated with better clinical outcomes and improved patient survival in response to ICI therapy. The association between T_{PEX} and improved efficacy of checkpoint blockade is further supported by our data, and importantly, that rhIL-7-hyFc effectively increases T_{PEX} to enhance checkpoint blockade.

A recent study showed that long-term proliferative potential, multipotency and repopulation capacity of

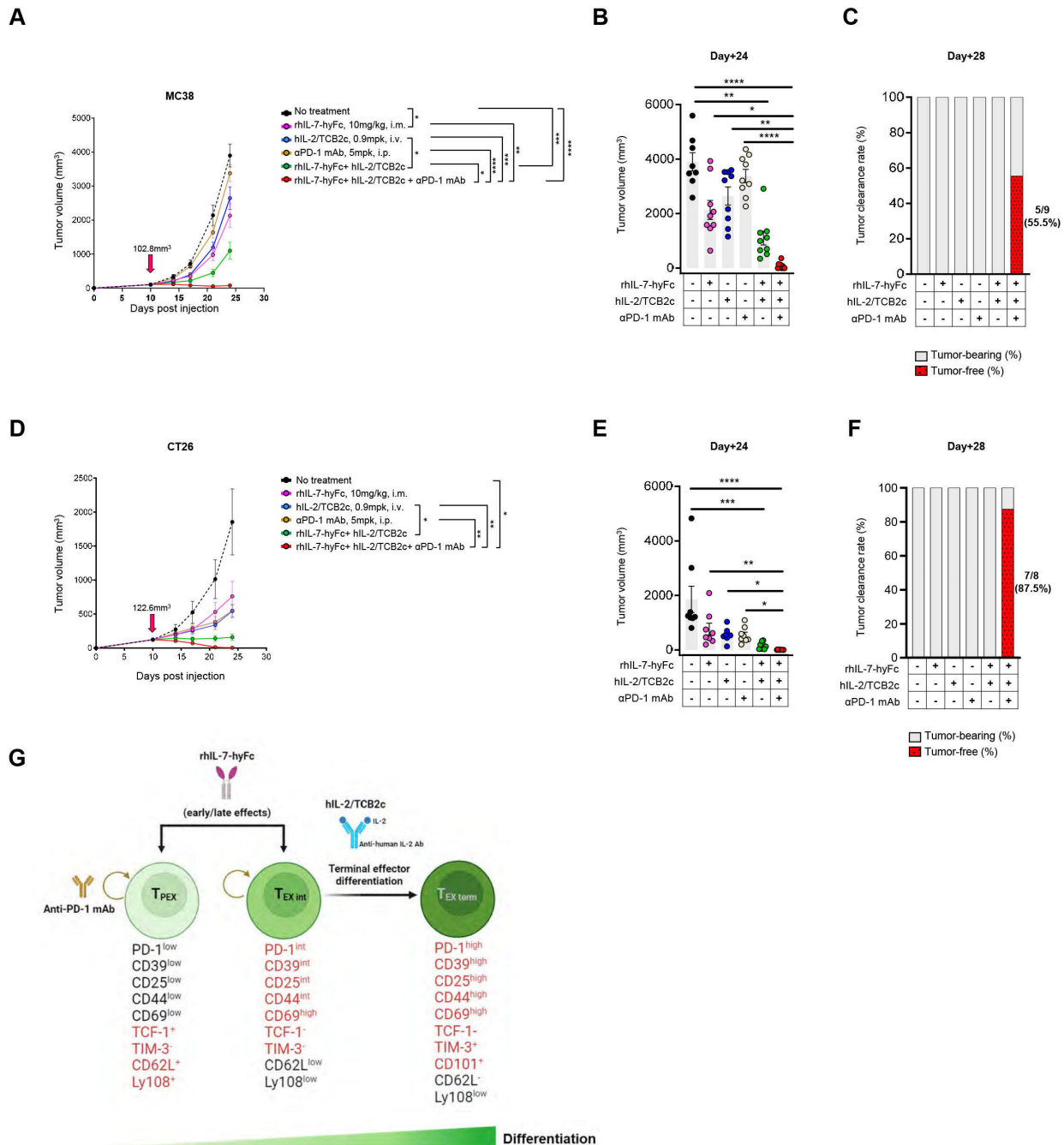


Figure 7 rhIL-7-hyFc and hIL-2/TCB2c improves the antitumor efficacy of PD-1 blockade therapy, achieving complete regression of tumor. MC38 cells (5×10^5 cells/mouse) subcutaneously implanted into the mice and when the volume reached approximately 100 mm^3 , the mice were randomly allocated to either the control or treatment groups ($n=9$ per group). 10 mg/kg rhIL-7-hyFc or 0.9 mg/kg hIL-2/TCB2c was administered intramuscularly (i.m.) and intravenously (i.v.). The α PD-1 mAb was administered by intraperitoneal (i.p.) injection every 3 days for a total of three injections. (A) Average growth curves of MC38 tumors treated with indicated regimens. (B) Tumor volumes on indicated day post implant. (C) Pooled data showing the percentage of tumor-free (red with black dots) or tumor-bearing (gray) mice on day 28. The number of tumor-free mice out of the total animals is indicated below each bar. In a syngeneic CT26 model, mice were inoculated subcutaneously with 3×10^5 tumor cells, and when the tumor size reached approximately 120 mm^3 , treatment was initiated using the same dose and treatment schedule employed in the MC38 tumor model. (D) Tumor growth curves of CT26 after different treatment regimens ($n=8$ per group). Tumor volumes (E) and the percentage of tumor-free mice (F) on indicated day. (G) Schematic illustration depicting the suggested mechanism of action of rhIL-7-hyFc, hIL-2/TCB2c, and anti-PD-1 mAb triple combination therapy. Graphs show mean \pm SEM. Data were analyzed by two-way (A, D) or one-way (B, E) analysis of variance with Turkey's testing for multiple comparisons. Statistical significance is indicated as * $p < 0.05$, ** $p < 0.01$, *** $p < 0.001$, **** $p < 0.0001$. i.m., intramuscularly; i.p., intraperitoneal; i.v., intravenously; mAb, monoclonal antibody; PD-1, programmed cell death protein 1; rhIL, recombinant human interleukin; TCF-1, T cell factor 1; T_{EX int}, intermediate exhausted T cell; T_{EX term}, terminally exhausted T cell; TIM-3, T cell immunoglobulin and mucin domain-3; T_{PEX}, progenitor exhausted T cell.

exhausted T cells during chronic infection are selectively preserved in a small population of CD62L⁺Ly108⁺ T_{PEX} cells.²⁴ Intriguingly, the administration of rhIL-7-hyFc resulted in an increase of CD62L⁺Ly108⁺ T_{PEX} cells in the tumor as well as peripheral compartments. Concomitantly, rhIL-7-hyFc resulted in the proliferation of T_{PEX} cells in tdLNs. Previous studies have indicated that T_{PEX} cells in the TME originate from tdLNs.^{32,33} Therefore, the increased numbers of early CD8⁺ T_{PEX} cells in rhIL-7-hyFc-treated tumors may likely originate from tdLNs.

In multiple cancer types, the majority of tumor-derived TIM-3⁺CD4 T cells express higher levels of CD25 and Foxp3.³⁴ Importantly, TIM-3⁺ Treg cells tend to exhibit a more suppressive phenotype compared with TIM-3⁻ Treg.³⁵ Recent studies have suggested that the presence of TIM-3⁺ Treg cells in the TME is associated with unfavorable prognoses in patients with cancer. In line with these findings, higher frequencies of TIM-3⁺ Tregs have been correlated with tumor progression, metastasis, and resistance to immunotherapy.^{36,37} It is noteworthy that rhIL-7-hyFc led to a significant reduction in the frequencies of CD39^{high} TIM-3⁺ Treg cells in tumors. Additionally, our previous study demonstrated that rhIL-7-hyFc effectively diminishes the number of MDSCs.¹⁴ Collectively, these findings suggest that rhIL-7-hyFc holds potential as a therapeutic agent for modulating the TME towards an immunostimulatory milieu by decreasing immunosuppressive cells such as MDSCs and CD39^{high} TIM-3⁺ Tregs.

In this study, we describe that a triple combination with rhIL-7-hyFc, hIL-2/TCB2c, and PD-1 inhibitor shows a more robust antitumor efficacy, achieving complete regression of tumor lesions. This suggests that rhIL-7-hyFc and hIL-2/TCB2c synergize with anti-PD-1 to improve antitumor efficacy. This effect is potentially facilitated by increasing the population of cells that are likely responsive to anti-PD-1 therapy.

Previous research has shown that the combination therapy of PD-1 and IL-2, unlike PD-1 monotherapy, induces a significant alteration in the differentiation program of T_{PEX} cells when CD25 engagement is preserved. This combination therapy results in the generation of highly functional effector CD8⁺ T cells displaying distinct transcriptional and epigenetic profiles during chronic viral infections.³⁸ While the hIL-2/TCB2c we used in this study avoids CD25 engagement, its combination with rhIL-7-hyFc shows clear synergistic effects. It is tempting to speculate even higher synergistic effects when rhIL-7-hyFc is combined with IL-2 candidates that retain CD25 engagement, as previous studies have shown that better effector cells express high IL-7R. However, it is well-known that the constitutive expression of CD25 on Treg and certain endothelial cells can lead to undesired systemic effects associated with IL-2 therapy.

To address this issue, a novel approach involving the cis binding of PD-1-IL2v to PD-1 and IL-2Rβγ on the same cell has been developed.^{39,40} This strategy allows for the differentiation of stem-like CD8⁺ T cells into superior effector cells in cancer models, without the need for

CD25 binding. As a result, this strategy offers enhanced efficacy while minimizing systemic effects associated with IL-2 therapy. The presence of IL-7R on superior effector cells induced by PD-1-IL2v suggests the possibility of a synergistic effect with rhIL-7-hyFc, potentially leading to enhanced antitumor efficacy. This combined approach holds great promise for augmenting the activation, proliferation, and functionality of PD-1⁺CD8⁺ T cells, thereby bolstering the immune response against cancer cells.

MATERIALS AND METHODS

Animal experiments

C57BL/6/J and BALB/c female mice (6–7 weeks) were purchased from Daehan Bio Link (DBL) and subsequently habituated under specific pathogen-free conditions at the animal facility of Pohang University of Science and Technology (POSTECH). C57BL/6 mice were subcutaneously injected with 5×10⁵ MC38 cells into the right flank, while BALB/c mice were subcutaneously injected with 3×10⁵ CT26 cells into the right flank. Mice were randomized into treatment groups to equalize tumor volume within groups. The hIL-2/TCB2c was administered intravenously at a single dose of 0.9 mg/kg, hIL-7-hyFc was administered intramuscularly at a single dose of 10 mg/kg. Anti-mouse PD-1 monoclonal antibody (Bio X Cell, #BE0273, clone 29F.1A12) was administered intraperitoneally three times with a 3-day interval, at a dose of 5 mg/kg. Tumor size was measured using digital calipers, and tumor volume was determined using the formula (A²×B)/2, where A represents the shortest diameter and B represents the longest diameter of the tumor. Tumor volumes were measured twice a week. Animals with conditions exceeding the following humane endpoints for tumor size were euthanized: a tumor diameter measuring greater than 20 mm in any single dimension.

Cell lines

The murine colon carcinoma, MC-38 cell line was kindly provided by Professor Seung-Woo Lee (Department of Life Sciences, POSTECH). MC-38 cells were grown in Dulbecco's Modified Eagle Medium (Welgene, #LM001-05) supplemented with 10% Fetal Bovine Serum (Hyclone, #SV30207.02), 1% penicillin–streptomycin (Thermo Fisher, #15140122) and subculture with 0.25% trypsin-EDTA (Gibco, #25200072). The CT-26 (ATCC CRL-2638) cell line was purchased from American Type Culture Collection. CT-26 cells were grown in Roswell Park Memorial Institute media (RPMI 1640; Welgene, #LM011-51) supplemented with 10% FBS, 1% penicillin–streptomycin and digested with 0.25% trypsin-EDTA for subculture. All cell lines were maintained 37°C in 5% CO₂.

Cell preparation

The isolated tumors were weighed to calculate the absolute number of cells relative to the tumor weight. To obtain a single-cell suspension, tumor samples were

finely chopped and dissociated using enzymatic cocktails composed of 400 U/mL-1 Collagenase D (Sigma-Aldrich, #11088866001) and 20 U/mL-1 DNase (Sigma-Aldrich, #04536282001) at 37°C for 30 min for digestion. TdLN tissue was minced to obtain single-cell suspension. The digested tumor and the minced lymph node were then passed through a 40 µm cell strainer (SPL Life Sciences #93040). Peripheral blood was collected from tumor-bearing mice using the retroorbital bleeding route, and blood was collected into a K3-EDTA (Greiner Bio-One International GmbH, #450530) tube to prevent clotting. RPMI+10% FBS was added to dilute out the anti-coagulant, and then white blood cells were separated from red blood cells using centrifugation. The cell count was determined using a Vi-CELL BLU (Beckman Coulter, #C19196).

Flow cytometry

An aliquot of 50 µL of cell suspension ($2\text{--}5 \times 10^6$ cells) was seeded into a 96-well plate. The single cells were stained with LIVE/DEAD Fixable Blue Dead Cell Stain Kit (Invitrogen, #L34962) to exclude dead cells and subsequently stained with anti-mouse CD16/32 (BioLegend, #101302) for 30 min at 4°C in phosphate buffered saline (PBS) and fluorescence-conjugated antibodies. Cells were stained with fluorescence-conjugated antibodies (see online supplemental table S1) in flow cytometry staining buffer with Brilliant Stain Buffer Plus (10 µL per test, BD Biosciences, #566385). Surface staining was performed for 1 hour at room temperature in flow cytometry staining buffer (PBS with 2% fetal bovine serum). Intracellular staining was performed using the FoxP3/transcription factor staining buffer set (Thermo Fisher, #00-5523-00). Intracellular staining was performed for 1 hour at room temperature. Samples were acquired by Cytex Aurora equipped with five lasers (Cytex Biosciences) and analyzed with SpectoFlow (V.3.0.3) and FlowJo software (V.10.8.1, Tree Star).

Statistical analysis

GraphPad Prism V.10 was used for all data analysis. Data were expressed as the mean±SEM or ±SD as stated in figure legends. The statistical test used in individual experiments is indicated in the figure legends. All data were evaluated using one-way or two-way analysis of variance with Tukey's multiple comparisons test. The level of significance was indicated as *, $p < 0.05$; **, $p < 0.01$; ***, $p < 0.001$; ****, $p < 0.0001$.

Acknowledgements The authors would like to thank Selectixine for providing the hIL-2/TCB2c. We also thank the members of the POSTECH animal facility for providing technical support.

Contributors ML: conceptualization, data curation, formal analysis, project administration, visualization, validation, writing—original draft. S-KI: project administration, supervision, writing—original draft. SB: data curation, project administration. MJ, MK, E.J.L, and STJ: investigation, methodology, project administration, resources. SF-M and AW: writing—review and editing. J-YL and DK: material support. DC: guarantor, conceptualization, project administration, supervision, writing—review and editing. All authors contributed to the article and approved the final manuscript.

Funding The authors have not declared a specific grant for this research from any funding agency in the public, commercial or not-for-profit sectors.

Competing interests ML, S-KI, SB, MJ, MK, E.J.L, STJ, SF-M, AW and DC are currently employed by NeolmmuneTech. J-YL and DK work for Selectixine.

Patient consent for publication Not applicable.

Ethics approval All animal experiments were in accordance with protocols approved by the Institutional Animal Care and Use Committees of the POSTECH (POSTECH-2022-0066).

Provenance and peer review Not commissioned; externally peer reviewed.

Data availability statement Data are available upon reasonable request. All data relevant to the study are included in the article or uploaded as supplementary information. Data are available upon reasonable request.

Supplemental material This content has been supplied by the author(s). It has not been vetted by BMJ Publishing Group Limited (BMJ) and may not have been peer-reviewed. Any opinions or recommendations discussed are solely those of the author(s) and are not endorsed by BMJ. BMJ disclaims all liability and responsibility arising from any reliance placed on the content. Where the content includes any translated material, BMJ does not warrant the accuracy and reliability of the translations (including but not limited to local regulations, clinical guidelines, terminology, drug names and drug dosages), and is not responsible for any error and/or omissions arising from translation and adaptation or otherwise.

Open access This is an open access article distributed in accordance with the Creative Commons Attribution Non Commercial (CC BY-NC 4.0) license, which permits others to distribute, remix, adapt, build upon this work non-commercially, and license their derivative works on different terms, provided the original work is properly cited, appropriate credit is given, any changes made indicated, and the use is non-commercial. See <http://creativecommons.org/licenses/by-nc/4.0/>.

ORCID iD

Minji Lee <http://orcid.org/0000-0003-2957-4457>

REFERENCES

- Rosenberg SA. IL-2: the first effective immunotherapy for human cancer. *J Immunol* 2014;192:5451–8.
- Overwijk WW, Tagliaferri MA, Zalevsky J. Engineering IL-2 to give new life to T cell immunotherapy. *Annu Rev Med* 2021;72:281–311.
- Katre NV, Knauf MJ, Laird WJ. Chemical modification of recombinant interleukin 2 by polyethylene glycol increases its potency in the murine METH A sarcoma model. *Proc Natl Acad Sci U S A* 1987;84:1487–91.
- Boyman O, Kovar M, Rubinstein MP, et al. Selective stimulation of T cell subsets with antibody-cytokine immune complexes science. *Science* 2006;311:1924–7.
- Sharma M, Khong H, Fa'ak F, et al. Bempegaldesleukin selectively depletes intratumoral Tregs and potentiates T cell-mediated cancer therapy. *Nat Commun* 2020;11:661.
- Sim GC, Martin-Orozco N, Jin L, et al. IL-2 therapy promotes suppressive ICOS+ Treg expansion in melanoma patients. *J Clin Invest* 2014;124:99–110.
- Lee J-Y, Lee E, Hong S-W, et al. Tcb2, a new anti-human interleukin-2 antibody, facilitates heterodimeric IL-2 receptor signaling and improves anti-tumor immunity. *Oncoimmunology* 2020;9:1681869.
- Pellegrini M, Calzascia T, Elford AR, et al. Adjuvant IL-7 antagonizes multiple cellular and molecular inhibitory networks to enhance immunotherapies. *Nat Med* 2009;15:528–36.
- Schroten-Loef C, de Ridder CMA, Reneman S, et al. A prostate cancer vaccine comprising whole cells secreting IL-7, effective against subcutaneous challenge, requires local GM-CSF for intra-prostatic efficacy. *Cancer Immunol Immunother* 2009;58:373–81.
- Mackall CL, Fry TJ, Gress RE. Harnessing the biology of IL-7 for therapeutic application. *Nat Rev Immunol* 2011;11:330–42.
- Choi YW, Kang MC, Seo YB, et al. Intravaginal administration of FC-fused I17 suppresses the Cervicovaginal tumor by recruiting HPV DNA vaccine-induced Cd8 T cells. *Clin Cancer Res* 2016;22:5898–908.
- Campian JL, Ghosh S, Kapoor V, et al. Long-acting recombinant human interleukin-7, NT-17, increases cytotoxic Cd8 T cells and enhances survival in mouse glioma models. *Clin Cancer Res* 2022;28:1229–39.
- O'Neal J, Cooper ML, Ritchey JK, et al. Anti-myeloma efficacy of CAR-iNKT is enhanced with a long-acting IL-7. *Blood Advances* 2023;7:6009–22.

- 14 Kim J, Kim Y, Choi D, *et al.* Hybrid Fc-Fused Interleukin-7 induces an inflamed tumor Microenvironment and improves the efficacy of cancer Immunotherapy. *Clin & Trans Imm* 2020;9. 10.1002/cti2.1168 Available: <https://onlinelibrary.wiley.com/toc/20500068/9/9>
- 15 Kim MY, Jayasinghe R, Devenport JM, *et al.* A long-acting Interleukin-7, rhIL-7-hyFc, enhances CAR T cell expansion, persistence, and anti-tumor activity. *Nat Commun* 2022;13:3296.
- 16 Jie H-B, Gildener-Leapman N, Li J, *et al.* Intratumoral regulatory T cells Upregulate immunosuppressive molecules in head and neck cancer patients. *Br J Cancer* 2013;109:2629–35.
- 17 Shen P, Yue R, Tang J, *et al.* Preferential Tim-3 expression on Treg and Cd8+ T cells, supported by tumor-associated Macrophages, is associated with worse prognosis in gastric cancer. *Am J Transl Res* 2016;8:3419–28.
- 18 Ye X, Waite JC, Dhanik A, *et al.* Endogenous retroviral proteins provide an Immunodominant but not requisite antigen in a murine Immunotherapy tumor model. *Oncimmunology* 2020;9:1758602.
- 19 Sun Z, Ren Z, Yang K, *et al.* A next-generation tumor-targeting IL-2 preferentially promotes tumor-infiltrating Cd8(+) T-cell response and effective tumor control. *Nat Commun* 2019;10:3874.
- 20 Levin AM, Bates DL, Ring AM, *et al.* Exploiting a natural conformational switch to engineer an Interleukin-2 'Superkine' *Nature* 2012;484:529–33.
- 21 Miller BC, Sen DR, Al Aboys R, *et al.* Subsets of exhausted Cd8(+) T cells Differentially mediate tumor control and respond to Checkpoint blockade. *Nat Immunol* 2019;20:326–36.
- 22 Guo Y, Xie Y-Q, Gao M, *et al.* Metabolic Reprogramming of terminally exhausted Cd8(+) T cells by IL-10 enhances anti-tumor immunity. *Nat Immunol* 2021;22:746–56.
- 23 Buchwald ZS, Nasti TH, Lee J, *et al.* Tumor-draining lymph node is important for a robust Abscopal effect stimulated by radiotherapy. *J Immunother Cancer* 2020;8:e000867.
- 24 Tsui C, Kretschmer L, Rapelius S, *et al.* MYB Orchestrates T cell exhaustion and response to Checkpoint inhibition. *Nature* 2022;609:354–60.
- 25 Hudson WH, Gensheimer J, Hashimoto M, *et al.* Proliferating transitory T cells with an Effector-like transcriptional signature emerge from PD-1(+) stem-like Cd8(+) T cells during chronic infection. *Immunity* 2019;51:1043–58.
- 26 Im SJ, Konieczny BT, Hudson WH, *et al.* PD-1+ Stemlike Cd8 T cells are resident in Lymphoid tissues during persistent LCMV infection. *Proc Natl Acad Sci U S A* 2020;117:4292–9.
- 27 Wang D, Fang J, Wen S, *et al.* A comprehensive profile of Tcf1(+) progenitor and Tcf1(-) terminally exhausted PD-1(+)Cd8(+) T cells in head and neck squamous cell carcinoma: implications for prognosis and Immunotherapy. *Int J Oral Sci* 2022;14.
- 28 Held W, Siddiqui I, Schaeuble K, *et al.* Intratumoral Cd8(+) T cells with stem cell-like properties: implications for cancer Immunotherapy. *Sci Transl Med* 2019;11:eay6863.
- 29 Koh J, Kim S, Woo YD, *et al.* Tcf1(+)PD-1(+) tumour-infiltrating lymphocytes predict a favorable response and prolonged survival after immune Checkpoint inhibitor therapy for non-small-cell lung cancer. *Eur J Cancer* 2022;174:10–20.
- 30 Sade-Feldman M, Yizhak K, Bjorgaard SL, *et al.* Defining T cell States associated with response to Checkpoint Immunotherapy in Melanoma. *Cell* 2018;175:998–1013.
- 31 Im SJ, Hashimoto M, Gerner MY, *et al.* Defining Cd8+ T cells that provide the proliferative burst after PD-1 therapy. *Nature* 2016;537:417–21.
- 32 Connolly KA, Kuchroo M, Venkat A, *et al.* A reservoir of stem-like Cd8(+) T cells in the tumor-draining lymph node preserves the ongoing antitumor immune response. *Sci Immunol* 2021;6:eabg7836.
- 33 Rahim MK, Okholm TLH, Jones KB, *et al.* Dynamic Cd8(+) T cell responses to cancer Immunotherapy in human regional lymph nodes are disrupted in metastatic lymph nodes. *Cell* 2023;186:1127–43.
- 34 Yan J, Zhang Y, Zhang JP, *et al.* Tim-3 expression defines regulatory T cells in human tumors. *PLoS ONE* 2013;8:e58006.
- 35 Liu Z, McMichael EL, Shayan G, *et al.* Novel Effector phenotype of Tim-3(+) regulatory T cells leads to enhanced suppressive function in head and neck cancer patients. *Clin Cancer Res* 2018;24:4529–38.
- 36 Gao X, Zhu Y, Li G, *et al.* TIM-3 expression characterizes regulatory T cells in tumor tissues and is associated with lung cancer progression. *PLoS ONE* 2012;7:e30676.
- 37 Huang L, Xu Y, Fang J, *et al.* Targeting Stat3 Abrogates Tim-3 upregulation of adaptive resistance to PD-1 blockade on regulatory T cells of Melanoma. *Front Immunol* 2021;12:654749.
- 38 Hashimoto M, Araki K, Cardenas MA, *et al.* PD-1 combination therapy with IL-2 modifies Cd8(+) T cell exhaustion program. *Nature* 2022;610:173–81.
- 39 Ren Z, Zhang A, Sun Z, *et al.* Selective delivery of low-affinity IL-2 to PD-1+ T cells Rejuvenates antitumor immunity with reduced toxicity. *J Clin Invest* 2022;132:e153604.
- 40 Codarri Deak L, Nicolini V, Hashimoto M, *et al.* PD-1-cis IL-2R Agonism yields better effectors from stem-like Cd8(+) T cells. *Nature* 2022;610:161–72.